Novel poly(3-hydroxybutyrate) nanocomposites containing WS_2 inorganic nanotubes with improved thermal, mechanical and tribological properties

Mohammed Naffakh [a,*], Carlos Marco [b], Gary Ellis [b], Sidney R. Cohen [c], Alexander Laikhtman [d], Lev Rapoport [d], Alla Zak [d]

[a] Universidad Politécnica de Madrid, Departamento de Ingeniería y Ciencia de los Materiales, Escuela Técnica Superior de Ingenieros Industriales, José Gutiérrez Abascal 2, 28006 Madrid, Spain
[b] CSIC, Instituto de Ciencia y Tecnología de Polímeros (ICTP), Juan de la Cierva 3, 28006 Madrid, Spain
[c] Department of Chemical Research Support, Weizmann Institute of Science, Rehovot 76100, Israel
[d] Department of Sciences, Holon Institute of Technology, 52 Golomb St., Holon 58102, Israel

HIGHLIGHTS

- Environmentally-friendly INT–WS_2 is used to produce advanced PHB NCPs.
- Novel PHB NCPs are obtained without using modifiers or surfactants.
- Novel INT–WS_2 improve the thermal and mechanical properties of PHB.
- INT–WS_2 is effective in reducing the friction coefficient of PHB.
- The benefits of using INTs compared to other nanoscale fillers are highlighted.

GRAPHICAL ABSTRACT

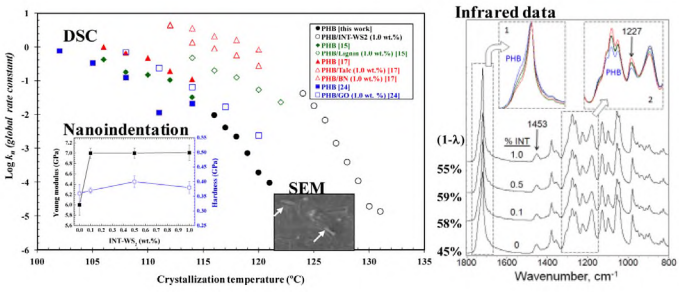

ABSTRACT

Poly(3-hydroxybutyrate) (PHB) nanocomposites containing environmentally-friendly tungsten disulphide inorganic nanotubes (INT–WS_2) have been successfully prepared by a simple solution blending method. The dynamic and isothermal crystallization studies by differential scanning calorimetry (DSC) demonstrated that the INT–WS_2 exhibits much more prominent nucleation activity on the crystallization of PHB than specific nucleating agents or other nanoscale fillers. Both crystallization rate and crystallinity significantly increase in the nanocomposites compared to neat PHB. These changes occur without modifying the crystalline structure of PHB in the nanocomposites, as shown by wide-angle X-ray diffraction (WAXS) and infrared/Raman spectroscopy. Other parameters such as the Avrami exponent, the equilibrium melting temperature, global rate constant and the fold surface free energy of PHB chains in the nanocomposites were obtained from the calorimetric data in order to determine the influence of the INT–WS_2 filler. The addition of INT–WS_2 remarkably influences the energetics and kinetics of nucleation and growth of PHB, reducing the fold surface free energy by up to 20%. Furthermore, these nanocomposites also show an improvement in both tribological and mechanical (hardness and modulus) properties with respect to pure PHB evidenced by friction and nanoindentation tests, which is of important potential interest for industrial and medical applications.

Keywords:
Composite materials
Nanostructures
Thermal properties
Mechanical properties
Tribology

* Corresponding author. Tel.: +34 913 363 164; fax: +34 913 363 007.
E-mail address: mohammed.naffakh@upm.es (M. Naffakh).

1. Introduction

Research into the industrial exploitation of products derived from renewable resources is currently of immense international importance. The development of such materials is receiving considerable attention, because the availability of crude oil could become severely restricted within the foreseeable future, and its replacement by renewable raw materials is consistent with the aims of global sustainability. This challenge motivates academic and industrial research efforts to develop novel "environmentally-friendly" materials produced from alternative resources, with lower energy consumption, biodegradability and low toxicity to the environment [1–3]. The degree of "friendliness" would be highest when all of these requisites are combined into the same material. Natural aliphatic polyesters are an attractive solution. These polymers can be easily converted into simpler compounds and mineralized. Thus, minimum environmental pollution is expected from post-use disposal of such materials, representing an interesting alternative to common non-degradable polymers for short-life span applications (packaging, agriculture, pharmacology, medicine, etc.) [4–7]. Nevertheless, until now most biopolymers are costly compared to conventional thermoplastics, and are structurally deficient for practical use. Therefore, strategies to improve the properties of these biopolymers to make them fully competitive with common thermoplastics are of significant current interest.

Among these biodegradable polymers, poly(3-hydroxybutyrate) (PHB) belongs to a family of poly(hydroxyalkanoates) (PHAs) that can be accumulated by a variety of bacteria as a reserve energy source [7–9]. PHB is a truly biodegradable and biocompatible polymer with relatively high melting point (ca. 180 °C) and crystallinity (>45%). However, practical applications of PHB are often limited by its brittleness and narrow processing window. There are several possible causes of this brittleness. For example, bacterially synthesized PHB is a completely isotactic stereoregular polyester with a high tendency to crystallize. However, the nucleation density of PHB is too low to initiate efficient crystallization. As a result, it forms extremely large sized spherulites. After the first-stage crystallization from the melt state, secondary crystallization occurs slowly at room temperature, which is partly attributed to a low glass-transition temperature (~5 °C). All these factors are interrelated and promote interspherulitic cracking during storage of the polymer at room temperature, severely impairing the mechanical properties of the materials [10]. Considerable progress has been made to enhance the mechanical and thermal properties of PHB by blending it with other polymers such as poly(lactide), poly(vinyl alcohol), poly(ethylene oxide), or poly[(3-hydroxybutyrate)-co-(3-hydroxyvalerate)] (PHBV) [11–13], by adding plasticizers, nucleating agents, processing aids, and/or through thermal annealing [14–20]. Recently, another approach to improve the mechanical properties has been the incorporation into the polymer matrix of small amounts (<10 wt.%) of nano-sized fillers, such as clays, carbon nanotubes or graphene) [6,21–24]. In these cases the final behavior can be considerably improved by good particle dispersion and the formation of strong and extensive polymer–nanofiller interactions. However, without proper chemical treatment to reduce the surface energy it is very common for the nanoparticles to form clusters or agglomerates. When this occurs, nanocomposite formation is limited, as are the property improvements.

For these reasons the use of alternative filler particle types, such as inorganic fullerenes and nanotubes (INTs) based on layered metal dichalcogenides of WS_2 and MoS_2 is proposed. The first synthesis of these nanoparticles was reported by Tenne at al. in 1992 and 1993 [25,26]. Since then the synthetic technology has improved considerably and nearly (>99%) pure materials are already available on an industrial scale [27,28]. The synthetic process is catalyst-free, and the precursors (eg. tungsten oxide and H_2S or sulfur) are relatively inexpensive. Therefore, the moderate cost of such nanostructures may afford potential applications in catalysis, rechargeable batteries, drug delivery, solar cells and electronics, and more recently, in the field of polymer nanocomposites [29]. In this respect, WS_2 nanotubes (INT–WS_2) have been used as reinforcing agents to improve the mechanical and tribological properties of epoxy composites [30], electrospun poly(methyl methacrylate) fibers [31] and poly(propylene fumarate) (PPF) nanocomposite [32]. Also, INT–MoS_2 have also shown a remarkable effect on the thermal and mechanical properties of isotactic polypropylene, after successful dispersion by means of the most simple, cost-effective and ecologically friendly processing method, i.e. the melt-processing route [33].

In this context, we have developed a new family of nanocomposites that comprise poly(3-hydroxybutyrate) (PHB) and environmentally friendly inorganic nanotubes (INT–WS_2) in order to explore new opportunities for the preparation and development of advanced biodegradable polymer nanocomposites [34]. The successful dispersion of INT–WS_2 induced a remarkable improvement in the dynamic crystallization behavior of PHB, without using modifiers or surfactants. The prime objective of this investigation is to address the structure–property–performance relationship of PHB/INT–WS_2. In particular, the effects of different INT–WS_2 loadings on the thermal, structural, mechanical and tribological properties of PHB in the nanocomposites were studied and discussed in detail.

2. Experimental section

2.1. Materials

The matrix biopolymer was poly(3-hydroxybutyrate) (PHB), obtained from Fluka Chemicals (Germany) and the inorganic nanotubes (INT–WS_2) with diameters between 30 and 150 nm and lengths between 1 and 20 μm were provided by NanoMaterials Ltd (Israel). Various formulations of PHB/INT–WS_2 nanocomposites were prepared by dispersing INT–WS_2 (0.1, 0.5 and 1 wt. %) in a solution of PHB in chloroform, then precipitated in methanol and subsequently filtered and dried in a vacuum oven at 50 °C for 24 h.

2.2. Instrumentation

Scanning electron microscopy (SEM) images were obtained with an ultra-high field-emission scanning electron microscope (FESEM) SU8000 (Hitachi Co., Japan). Thermogravimetric analysis (TGA) experiments were conducted on a TA Instruments Q50 thermobalance with a heating rate of 10 °C min^{-1} from 100 to 800 °C in inert (nitrogen) atmosphere. Differential scanning calorimetry (DSC) measurements were carried out on a Perkin Elmer DSC7/Pyris differential scanning calorimeter, under nitrogen atmosphere. To study the nonisothermal crystallization behavior of PHB and its nanocomposites, the samples (ca. 10 mg) were firstly heated to 190 °C and held for 5 min to eliminate any thermal history [35–37]. For isothermal crystallization, the samples were initially melted at 190 °C for 5 min and then rapidly cooled (64 °C min^{-1}) to the desired crystallization temperature (T_c). The kinetics of crystallization was evaluated from the evolution of the exotherms during crystallization using Pyris DSC7 kinetic software. After crystallization was completed, the melting temperatures (T_m) were determined by heating the samples at a rate of 5 °C min^{-1}. For the estimation of the crystallinity of the samples, the ratio between the apparent enthalpy (e.g. the integration of the exothermic curve) and the 100% crystalline melting enthalpy (i.e. 146 J g^{-1}) was used

[38]. Wide-angle X-ray diffraction (WAXS) diffractograms were obtained using a Bruker D8 Advance diffractometer (Bruker AXS GmbH, Karlsruhe, Germany) employing Ni-filtered CuKα radiation (λ = 1.5418 Å), over the angular region 2θ between 5 and 40°. Raman spectra were recorded in a Renishaw inVia Reflex Raman microscope using a 785 nm solid-state laser source and a 20× objective, with a laser power at the sample estimated between 0.1 and 2.0 mW. Infrared spectra were recorded at 4 cm^{-1} resolution in a Perkin Elmer i-Series IMAGE infrared microscope coupled to a System 2000 FTIR spectrometer. Nanomechanical tests were performed on dried PHB/INT−WS_2 nanocomposite films using an instrumented nanoindentation system (Agilent XP). The indenter was a 10 μm diameter spherical diamond tip, chosen to average out any small inhomogeneities in the sample. The tip was loaded into the sample at a strain rate of 0.05 s^{-1} using CSM (continuous stiffness measurement). The latter imposed a small (10 nm) modulation on the quasi static load, allowing continuous reading of both the hardness (H) and the modulus (E) as the load on sample was increased. Dry friction tests of the films were carried out using a ball-on-flat rig at temperature of about 24 °C and humidity of 50%. A standard steel ball-bearing with a diameter of 10 mm was slid against a flat sample of the polymer film for 1000 cycles. The measurements were carried out at sliding velocity of 1 mm s^{-1} and at a load of 20 g. Initial contact pressure calculated as Hertzian stress for the ideal spherical ball on the flat polymer surface was about 30 MPa. The roughness of the film surfaces prior to testing were determined using a Surtronic 3+ profilometer (Taylor−Hobson, Denmark). In addition, before and after the friction measurements an atomic force microscope (AFM) model DI3100 in the tapping mode, was also used to analyze the surface topography of the wear tracks of the nanocomposites.

3. Results and discussion

3.1. Morphology and thermal stability

It is well known that the level of dispersion of nanoreinforcements in a polymer matrix has an important influence on the thermal and mechanical properties of semicrystalline polymers. In Fig. 1, high-resolution SEM images of PHB/INT−WS_2 nanocomposites show that the INT−WS_2 are well-dispersed into the PHB matrix without any apparent aggregation. The INT−WS_2 do not require exfoliation or modification, making it possible to obtain new biopolymer nanocomposite formulations without the complexity and processing costs associated with such treatments.

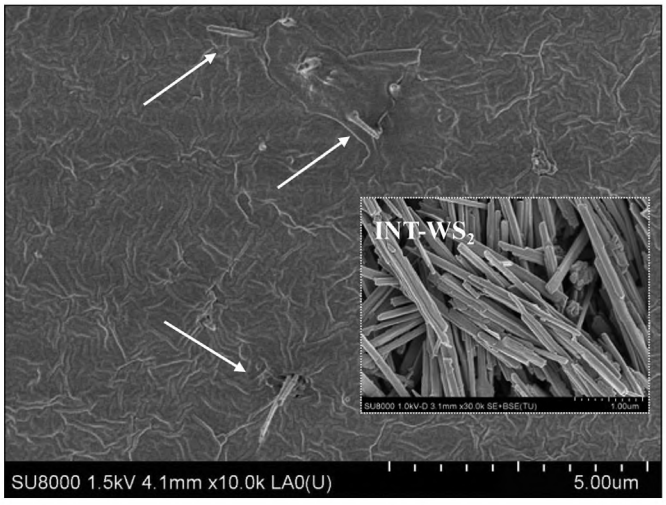

Fig. 1. High-resolution SEM image of PHB/INT−WS_2 (1.0 wt.%) nanocomposites.

As nanofillers generally affect the thermal stability of nanocomposites, thermogravimetric analysis (TGA) of the PHB/INT−WS_2 nanocomposites was carried out to establish the limiting processing conditions. The addition of INTs may result in an improvement of the heat resistance of the polymer matrix due to their high inherent thermal stability [31,33]. However, analysis of the thermogravimetric TGA curves revealed that the INT−WS_2 had no influence on the characteristic degradation temperatures of PHB, such as the temperature for 10% weight loss (T_{10}) and that corresponding to the maximum rate of weight loss (T_{mr}), which appeared at 286 °C and 303 °C, respectively.

3.2. Isothermal crystallization

The crystallization behavior of biodegradable polymers has fundamentally importance since it conditions not only the crystalline structure and morphology of the semicrystalline polymer, but also its final physical properties and biodegradability. The completion of isothermal crystallization inside the pre-heated mold over a short cycle period is very important for the efficient processing of high performance PHB materials (e.g. during injection molding). In this regard, the isothermal crystallization behavior of PHB/INT−WS_2 nanocomposites was explored. Fig. 2 shows the evolution of the heat flow versus crystallization time for the neat PHB and PHB/INT−WS_2 (1.0 wt.%) at different crystallization temperatures (T_c). As the crystallization temperature increased, the exotherms shifted along the time axis. Both the induction time and the width of the exotherms increased, reflecting a reduction in the crystallization rate of the system with decreasing undercooling (ΔT). The influence of T_c on crystallization is similar for both PHB and the nanocomposites, as shown in Fig. 2a and b. However, adding INT−WS_2 induces a remarkable shift of the crystallization range of PHB by around 10 °C (e.g. from 116 to 121 °C for PHB and from 124 to 131 °C for PHB/INT−WS_2 (1.0 wt.%)). Also, adding INT−WS_2 shortens the time to reach the maximum degree of crystallization, which means an increase in the crystallization rate. These results indicate that INT−WS_2 acted as a nucleation agent for PHB.

The crystalline transformation or conversion at time t, $\theta(t)$, can be defined as follows:

$$\theta(t) = \frac{\int_0^t \frac{dH(t)}{dt}dt}{\int_0^{t\infty} \frac{dH(t)}{dt}dt} = \frac{\Delta H_t}{\Delta H_\infty} \quad (1)$$

where dH/dt is the heat flow rate; ΔH_t is the heat generated at time t; ΔH_∞ is the total heat generated up to the end of the crystallization process. The rate of crystallization (G) was analyzed using the values of $\tau_{0.1}$ that corresponds to the time necessary to reach a degree of crystalline transformation of 10%. This parameter represents the global crystallization rate for each crystallization temperature, considering that $G \sim 1/\tau_{0.1}$. A pronounced change in the crystallization rate was observed as the temperature increased, in other words, as the undercooling decreased, Fig. 3. Also the apparent increase in the isothermal crystallization rate of PHB on the addition of INT−WS_2 in the PHB/INT−WS_2 nanocomposites, shown previously by comparison of the crystallization exotherms, was now exhibited over the full temperature range analyzed. In particular, the crystallization rate of PHB increased strongly with

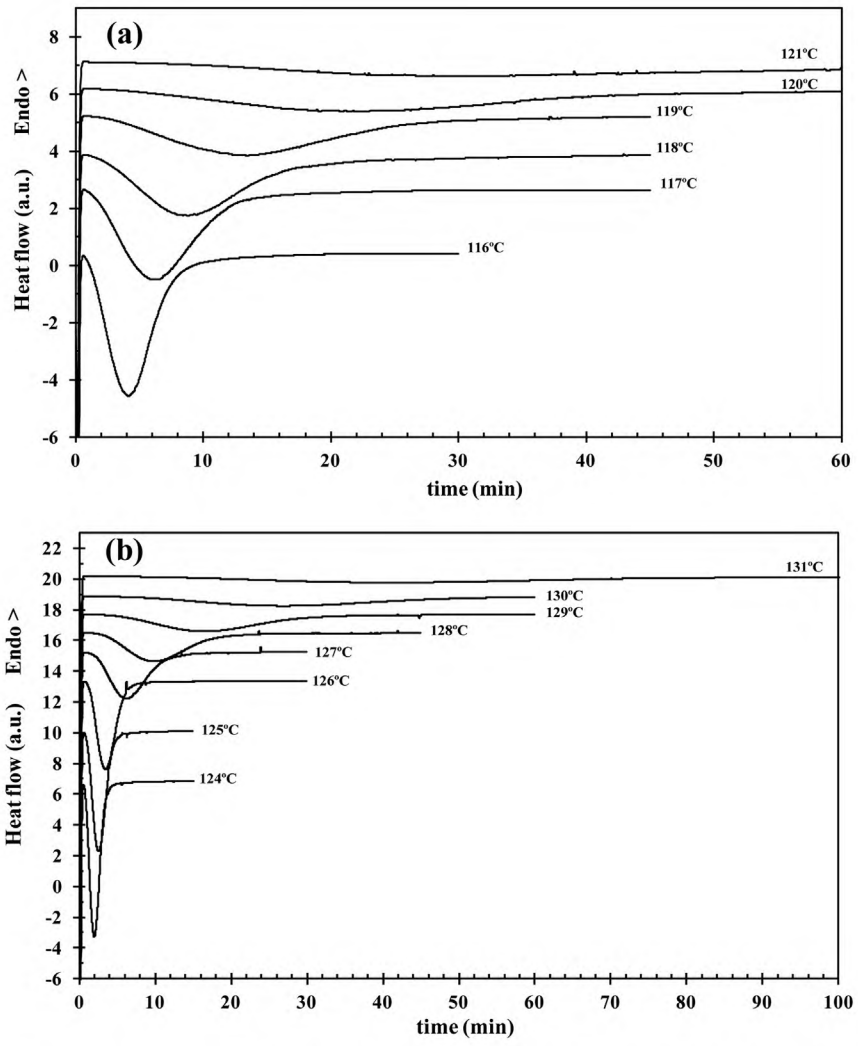

Fig. 2. DSC thermograms of isothermal crystallization of (a) PHB and (b) PHB/INT–WS_2 obtained at the indicated crystallization temperatures.

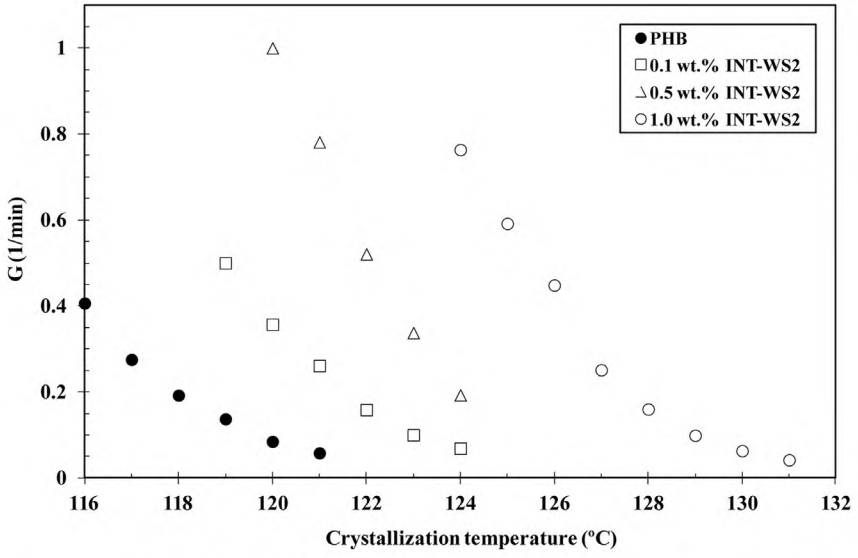

Fig. 3. Variation of the rate of crystallization (G) of PHB/INT–WS_2 nanocomposites as a function of the crystallization temperature (T_c).

composition suggesting that the well-dispersed INT−WS_2 remarkably enhance the nucleation of PHB.

The Avrami equation is further used to analyze the isothermal melt crystallization kinetics of neat PHB and its nanocomposites. This approximation assumes that the crystalline transformation or conversion (θ) develops with the crystallization time (t) as [39–41]:

$$\theta_t(t) = 1 - \exp(-kt^n) \quad (2)$$

where n is the Avrami exponent related to the type of nucleation and to the geometry of the growing crystals and k is the overall (macroscopic) rate constant (i.e. it contains contributions from both nucleation and growth). The above Eq. (2) can also be rewritten as follows:

$$\log[-\ln(1-\theta_t)] = \log k_n + n \log t \quad (3)$$

Linear regression of these straight lines at low degrees of crystalline transformation (5–25%) yields the Avrami exponents, n (Table 1). The average values obtained varied with the INT−WS_2 concentration as follows: $n \approx 2.6$ for neat PHB, $n \approx 3$ for PHB/INT−WS_2 (0.1 wt. %), $n \approx 3.2$ PHB/INT−WS_2 (0.5 wt. %) and $n \approx 3.3$ for PHB/INT−WS_2 (1.0 wt. %). According to the Avrami equation in the ideal state of nucleated crystallization for three-dimensional crystal growth, the value of the exponent should be exactly $n = 3$ [40]. However, during the actual process of crystal growth, the practical circumstances cannot satisfy the ideal state resulting in a deviation of the n value from 3, probably due to the existence of a thermal crystallization during the crystallization process [17].

Another important parameter determined from the crystallization kinetics was the global rate constant of the crystallization process (k_n), which can be determined by the following expression [42]:

$$k_n = \frac{\ln 2}{(\tau_{0.5})^n} \quad (4)$$

where $\tau_{0.5}$ is the time needed to reach 50% crystalline transformation. Values of k_n obtained for both neat PHB and its nanocomposites are summarized in Table 1, from which the effect of the crystallization temperature (T_c) and INT−WS_2 loading on the overall crystallization rate can be clearly seen. The values of k_n decrease with increasing T_c for both neat PHB and its nanocomposites with INT−WS_2. Such a trend indicates that the overall isothermal crystallization rate decreases with an increase of T_c, which is characteristic of nucleation controlled crystallization and associated with the proximity of the crystallization temperature to the melting temperature. However, the value of k_n for neat PHB is smaller than those of PHB/INT−WS_2 at the given temperatures. As an example, neat PHB presented a k_n of around 10×10^{-5} min^{-1} for T_c of 121 °C; in the case of the nanocomposites the k_n values at the same temperature change with the INT−WS_2 concentration as follows: 194×10^{-5} min^{-1} for 0.1 wt.% and 5566×10^{-5} min^{-1} for 0.5 wt.%. These results confirm the nucleating activity of the INT−WS_2 on the crystallization of PHB in isothermal conditions.

There is vigorous ongoing research attempting to discover efficient nucleating agents for PHB that increase the crystallization temperature and crystallization rates, as well as to generate smaller and more numerous spherulites leading to polymer materials with enhanced mechanical properties. Compounds ranging from talc [17], boron nitride (BN) [17,18], melamine [18], thyamine [18], cyclodextrin (α-CD) [16] and lignine [15] have been investigated as possible nucleating agents for PHB. In addition, some nano-sized fillers [23,24] such as carbon nanotubes and graphene oxide (GO) have also been shown to have the added advantage of acting as reinforcements for the polymer. Fig. 4 compares the variation of k_n values observed for PHB/INT−WS_2 composite with those obtained for PHB containing similar amounts (1.0 wt.%) of nucleating agents and/or nano-sized reinforcements. Clearly, INT−WS_2 induces a much more significant shift of the overall crystallization rate ranges of PHB along the crystallization temperature axis. This comparison indicates that INT−WS_2 has a more prominent nucleation activity on the crystallization of PHB than any other specific nucleating agent or nano-sized filler.

Table 1
Isothermal crystallization parameters of PHB and PHB/INT−WS_2: n = Avrami exponent and k = rate constant.

Sample	T_c (°C)	n	$k \times 10^5$
PHB	116	2.8	1109
PHB	117	2.6	484
PHB	118	2.5	234
PHB	119	2.5	87
PHB	120	2.6	19
PHB	121	2.5	10
PHB/INT−WS_2 (0.1 wt.%)	119	3.0	1674
PHB/INT−WS_2 (0.1 wt.%)	120	3.0	555
PHB/INT−WS_2 (0.1 wt.%)	121	3.0	194
PHB/INT−WS_2 (0.1 wt.%)	122	2.8	63
PHB/INT−WS_2 (0.1 wt.%)	123	2.9	8
PHB/INT−WS_2 (0.1 wt.%)	124	3.0	2
PHB/INT−WS_2 (0.5 wt.%)	119	3.9	29,047
PHB/INT−WS_2 (0.5 wt.%)	120	3.7	11,907
PHB/INT−WS_2 (0.5 wt.%)	121	3.4	5566
PHB/INT−WS_2 (0.5 wt.%)	122	3.1	1745
PHB/INT−WS_2 (0.5 wt.%)	123	2.8	675
PHB/INT−WS_2 (0.5 wt.%)	124	2.6	204
PHB/INT−WS_2 (1.0 wt.%)	124	3.8	4533
PHB/INT−WS_2 (1.0 wt.%)	125	3.6	2077
PHB/INT−WS_2 (1.0 wt.%)	126	3.5	799
PHB/INT−WS_2 (1.0 wt.%)	127	3.2	161
PHB/INT−WS_2 (1.0 wt.%)	128	3.1	46
PHB/INT−WS_2 (1.0 wt.%)	129	3.0	13
PHB/INT−WS_2 (1.0 wt.%)	130	3.1	2
PHB/INT−WS_2 (1.0 wt.%)	131	2.9	1

3.3. Melting behavior and equilibrium melting point

It was reported that the crystallization of PHB is slow and incomplete, while melting is complex due to superimposed melting–recrystallization–remelting processes [43]. Fig. 5 shows the DSC melting curves obtained in this study after isothermal crystallization at different T_c for PHB and the nanocomposites, where a triple melting behavior was observed. It is clear that as well as INT−WS_2 the crystallization temperature has a significant effect on the melting behavior of the polymer matrix after isothermal crystallization. As can be seen in Fig. 5, the first and second melting peaks (denominated T_{mI} and T_{mII}) for both neat PHB and PHB/INT−WS_2 (1.0 wt.%) shift to higher temperature with increasing T_c, which may be related to the perfection of the pre-existing PHB crystals formed at T_c. Thus, as a consequence, there is a disappearance the third melting endotherm (denominated T_{mIII}) of PHB/INT−WS_2 (1.0 wt.%) at the expense of T_{mII}, which is commonly assigned to recrystallized material (i.e. melting-recrystallization-melting of the original crystals of lower size or perfection and fusion of those originated during heating). However, the most relevant result was the disappearance of T_{mIII} for PHB/INT−WS_2, due to the fact that the strong nucleation effect of INT−WS_2 accelerates the crystallization of PHB in the nanocomposites. Therefore, the crystals formed in the

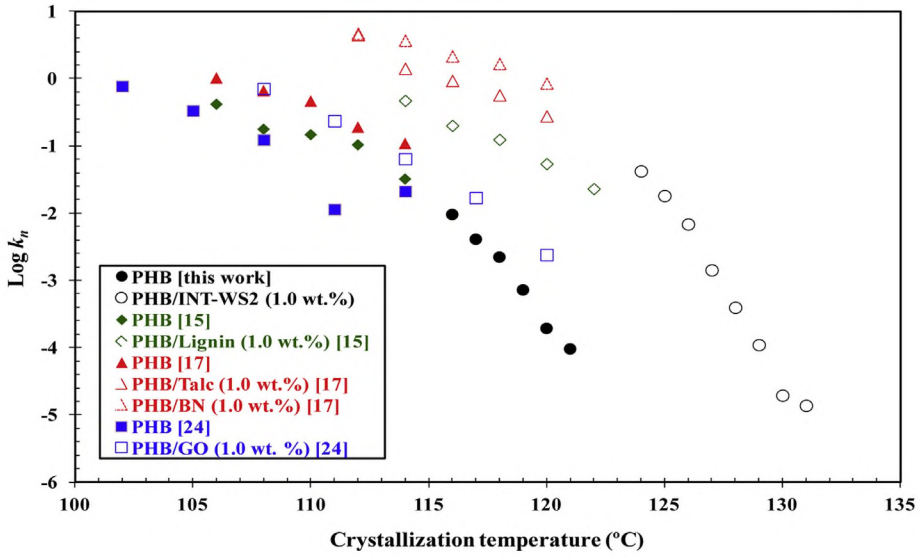

Fig. 4. Logarithmic plots of the global rate constant (k_n) of PHB systems containing same amounts of fillers (1.0 wt.%) as a function of the crystallization temperature (T_c).

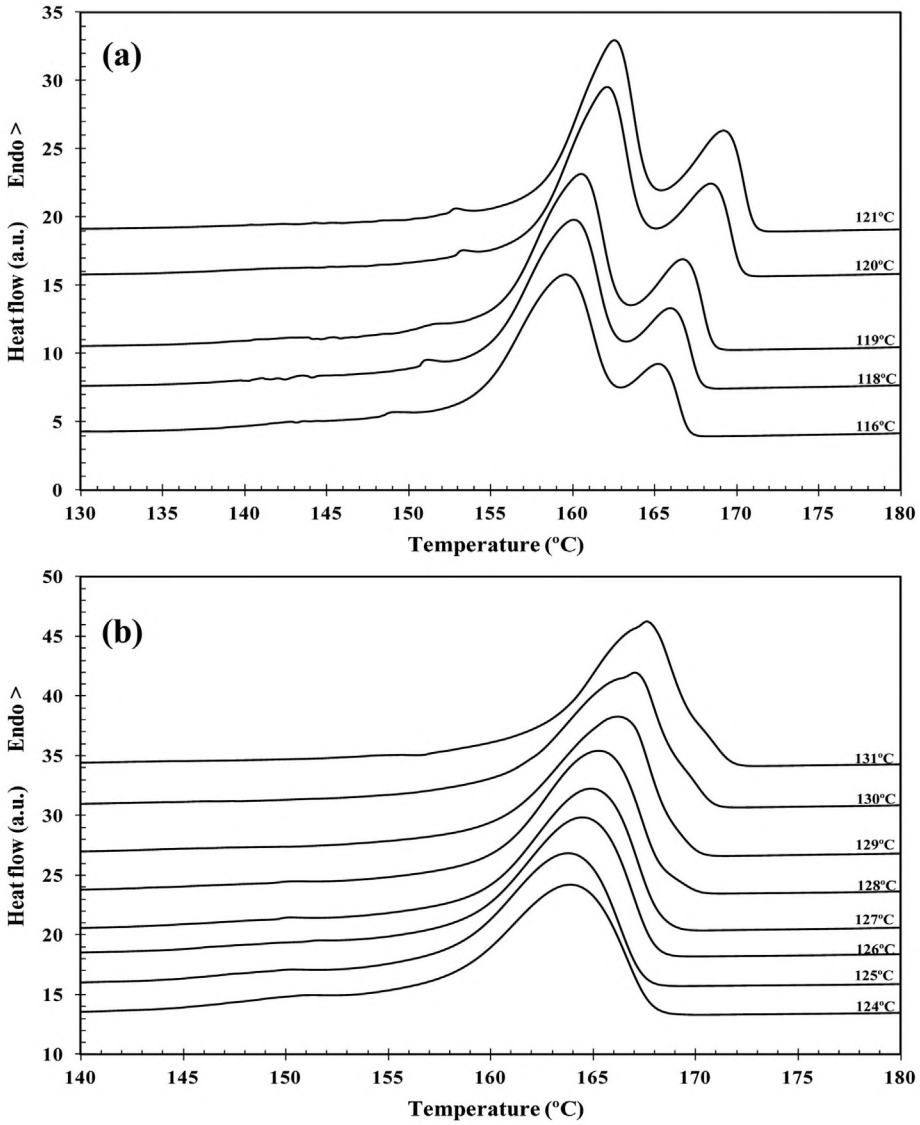

Fig. 5. DSC thermograms of (a) PHB and (b) PHB/INT–WS_2 (1.0 wt.%) obtained at a heating rate of 5 °C min^{-1} after isothermal crystallization at the indicated temperatures.

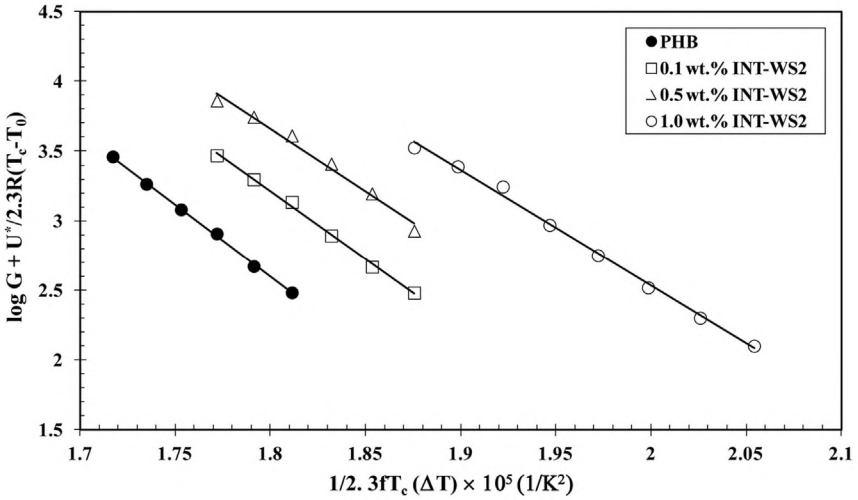

Fig. 6. Logarithmic plots of Eq. (5) for PHB/INT–WS_2 nanocomposites.

nanocomposites are more perfect and stable than those in neat PHB when the same crystallization temperature is used.

The kinetic data obtained by calorimetry were also analyzed from a thermodynamic point of view. The equilibrium melting point (T_m°) is obtained by conventional extrapolation of the resulting straight line to intersect of the representation $T_m = T_c$ [44]. Under this approximation, the extrapolation of the variation of the apparent melting temperature (T_{mII}) of Fig. 5 to the line corresponding with $T_m = T_c$ with little dispersion led to a value of 187 °C, which we can consider as the T_m° for the PHB/INT–WS_2 nanocomposites.

3.4. Crystallization activation energy

The isothermal crystallization activation energy will be presented in order to understand the dependence of the crystallization rate of PHB with composition. When polymeric materials crystallize at low undercooling (i.e. high T_c) the crystallization rate increases with the undercooling. This implies that the crystallization process is controlled by the nucleation stage, i.e. by the free energy needed for the formation of a stable crystallite or the free energy of nucleation, ΔG^*.

The kinetic data obtained in Fig. 3 have been examined in terms of the kinetic theory of crystallization [45,46], where the general expression for the growth rate of a linear polymer crystal with folded chains is given by:

$$G = G_0 \exp\left[-\frac{U^*}{R(T_c - T_0)}\right] \exp\left[-\frac{K_g}{fT_c\Delta T}\right] \quad (5)$$

G_0 is a pre-exponential term, independent on temperature, U^* is the activation energy needed for chain movement, T_0 represents the temperature at which they are motionless (usually $T_0 = T_g - 30$ K), R is the universal gas constant, ΔT is the undercooling that corresponds to $T_m^\circ - T_c$ where T_m° is the equilibrium melting temperature, and f is a correction factor that takes into account the variation of the equilibrium melting enthalpy (ΔH_m°) with temperature, defined as $2T_c/(T_c + T_m^\circ)$.

From T_c (116° – 131 °C) and T°_m values, we can determine that the crystallization of PHB and PHB/INT–WS_2 nanocomposites occurred in crystallization regime III [47,48], and therefore the nucleation constant (K_g) can be expressed as [49]:

$$K_g = \frac{4b_0\sigma\sigma_e T_m^0}{k_B\Delta H_m^0} \quad (6)$$

where σ and σ_e are the free energies per unit area of the surfaces of the lamellae parallel and perpendicular to the chain direction, respectively, b_0 is the distance between two adjacent fold planes and k_B is the Boltzmann constant. For the optimization of the linearization of the data within the temperature range the preferred values of U^*, T_0, R, k_B, T_m°, b_0, ΔH_m°, and σ are 10,250 J mol^{-1} [47], 225 K [47], 8.32 × 10^7 J mol^{-1} K, 1.38 × 10^{-23} J K^{-1}, 460 K [this work], 5.8 A [48], 1.85 × 10^8 J m^{-3} [48], and 29 × 10^{-3} J m^{-2}, respectively [48]. Under these considerations, Fig. 6 shows the logarithmic representation of Eq. (5) for both neat PHB and PHB/INT–WS_2 nanocomposites. The growth rate data fit well to straight lines, supporting unique regime behavior. From the slope of these plots, the values of K_g were calculated and the values of σ_e were obtained from $\sigma\sigma_e$ by substituting K_g in Eq. (6), Table 2. The K_g of PHB is about 1040 × 10^3 K^2. With the addition of INT–WS_2, the value of K_g changed to 975 × 10^3 K^2 at 0.1 wt. % INT–WS_2 content, 901 × 10^3 K^2 at 0.5 wt.% INT–WS_2 content and 833 × 10^3 K^2 at 1.0 wt.% INT–WS_2 content, respectively. There is a clear tendency for K_g to decrease with INT–WS_2 content, which confirm the nucleating activity of the INT–WS_2 on the crystallization of PHB. In the same way, the σ_e values showed a similar trend with INT–WS_2 content, along with a 6–20% decrease in the fold surface free energy of PHB.

The free energy of nucleation, i.e. the free energy necessary for the formation of a nucleus of a critical size, is given by the expression:

$$\Delta G^* = \frac{4b_0\sigma\sigma_e T_m^0}{\Delta H_m^0 \Delta T} \quad (7)$$

Table 2
Values of the nucleation constant (K_g) and fold surface free energy (σ_e) of PHB/INT–WS_2.

INT–WS_2 (wt.%)	K_g (K^2) × 10^{-3}	σ_e (erg cm^{-2})
0	1040	85.9
0.1	975	80.6
0.5	901	74.5
1.0	833	69.8

ΔG^*, which increases with smaller undercooling, was lower for the INT−WS_2 nanocomposites than for neat PHB at the same crystallization temperature as shown in Fig. 7, which confirms that the energy barrier for nucleation is lowered in the presence of INT−WS_2 leading to an increase in the overall crystallization rate.

3.5. Nonisothermal crystallization

Different crystallization experiments were performed by varying the cooling rates between 1 and 20 °C min^{-1} [34]. It was observed that the crystallization peak temperature (T_p) is affected by the presence of the INTs, and this was clearly a function of composition showing a remarkable increase in T_p of around 35 °C for the PHB nanocomposite with only 0.1 wt.% of INT−WS_2. At higher INT−WS_2 content the value of T_p for PHB continues to rise and tends to stabilize for the highest concentrations of 0.5 and 1.0 wt.%, with increments of around 37 °C. On the other hand, the crystallinity increases by up to 31% with the INT−WS_2 content, from a value of 45% for PHB, to values of 58, 59 and 55% for the nanocomposites with 0.1 wt.%, 0.5 wt.% and 1.0 wt.%, respectively. The aforementioned results indicate that INT−WS_2 dramatically accelerates the nonisothermal crystallization process of PHB and behaves as a highly efficient nucleating agent. Fig. 8 compares the crystallization behavior observed for the PHB/INT−WS_2 composites with that of PHB containing similar amounts (1.0 wt.%) of nucleating agents and/or nano-sized reinforcements. The crystallization behavior was determined from the exothermic DSC curves obtained at 10 °C min^{-1} by analyzing the difference between the crystallization peak temperature (T_p) of the composite and that of the neat PHB matrix (ΔT_p). The value of $\Delta T_p \sim 36$ °C obtained for INT−WS_2 is higher than that of 32 °C observed for BN [18], and far exceeds the values observed for other promising nanofillers such as carboxyl-functionalized multiwalled carbon nanotubes (MWCNT) [23] and graphene oxide (GO) [24].

3.6. Crystalline structure

Wide-angle X-ray diffraction (WAXS) measurements were made to determine whether the addition of INT−WS_2 affects the crystal form of the PHB (Fig. 9). The results obtained from the room temperature WAXS diffractograms of PHB/INT−WS_2 nanocomposites show only the characteristic diffraction peaks of the orthorhombic

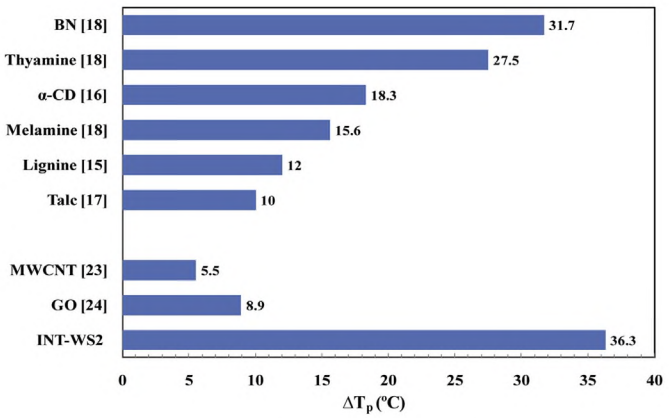

Fig. 8. Increment in the crystallization peak temperature (ΔT_p) of PHB systems containing some amounts of fillers (1.0 wt.%) obtained during cooling at 10 °C min^{-1}.

crystal form of PHB [50,51] and INT−WS_2 [27,52], demonstrating that the nanofiller does not influence the crystal structure of PHB.

Vibrational spectroscopy was also employed to study the materials, and in Fig. 10a the Raman spectra of PHB, INT−WS_2 and the PHB/INT−WS_2 nanocomposites are presented. Several characteristic bands were observed for the INT, particularly, the E^1_{2g} modes at around 355 and 383 cm^{-1} and the A_{1g} mode at around 421 cm^{-1} [53–55]. It is important to note that the INTs become sensitive to heating above 300 °C and the sulphide groups tend to convert to oxide in the presence of ambient oxygen [56]. The characteristic bands of the INT are clearly observed in the Raman spectra of the PHB/INT−WS_2 nanocomposites, and appear at the same frequencies as in the starting material, clearly suggesting that neither the processing conditions nor the sampling procedure have modified the structure of the INTs. The Raman spectra of the PHB matrix are little influenced by the incorporation of the INTs, independent of the composition. In Fig. 10b, infrared spectra for the PHB/INT−WS_2 nanocomposites are shown. The IR spectra, in contrast to Raman spectra, are sensitive to changes in both the crystal structure [57,58], and the degree of crystallinity. In the carbonyl stretching region there are two characteristic overlapping modes observed in all poly(hydroxyalkanoates) [59,60] that correspond to chains in crystalline and amorphous environments,

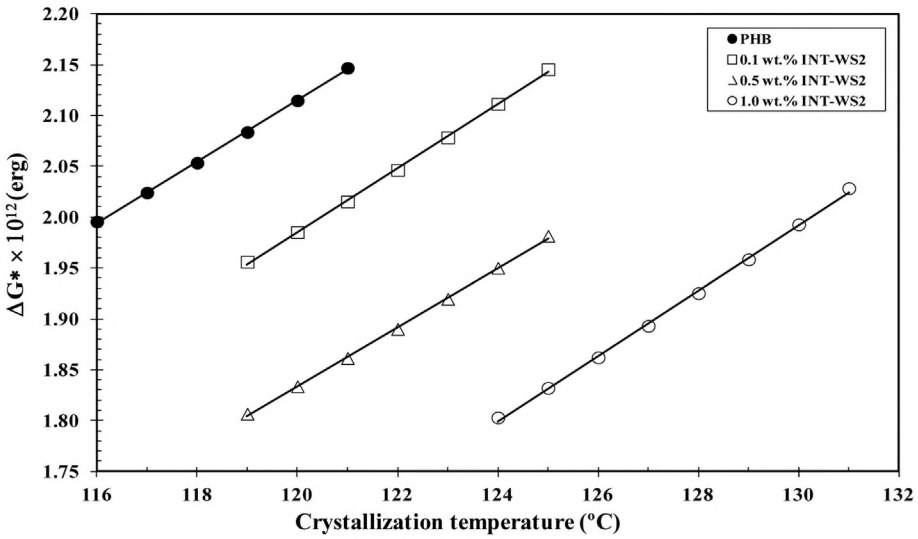

Fig. 7. Variation of the free energy of nucleation (ΔG^*) of PHB/INT−WS_2 nanocomposites as a function of the crystallization temperature (T_c).

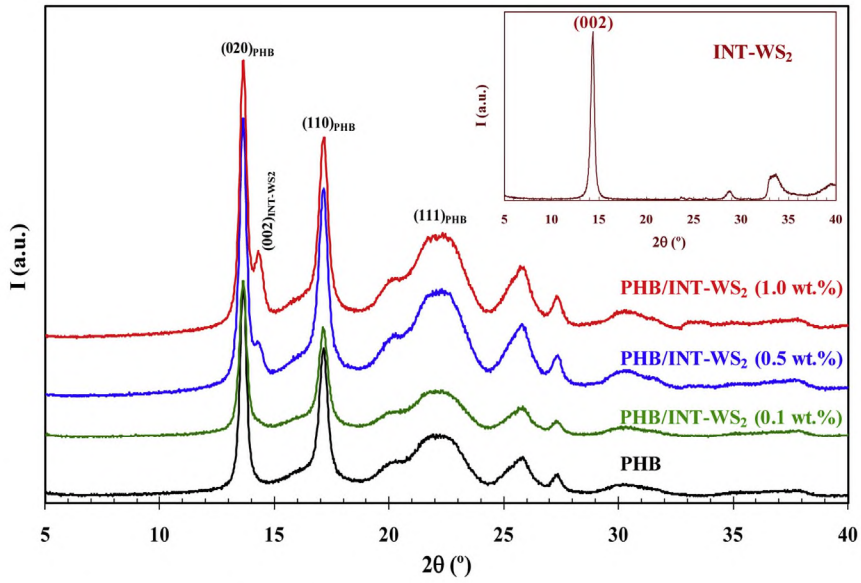

Fig. 9. WAXS diffractograms of PHB/INT–WS_2 nanocomposites obtained during cooling from the melt to room temperature at 10 °C min^{-1}; inset is the WAXS diffractogram of INT–WS_2.

appearing in PHB at approximately 1720 and 1740 cm^{-1}, respectively. The relative intensity of these two bands has been used to estimate crystallinity in PHAs [61] and can be seen to increase in all of the nanocomposites with respect to that of the neat PHB (PHB is the blue spectrum (in the web version) in inset 1 of Fig. 10b). The degree of crystallinity also affects the relative intensities of other bands, in particular the conformational CH_2 mode associated with helical chains in the crystals [62] that appears at around 1227 cm^{-1}, and is totally absent in the amorphous spectra. This mode has been compared to that of an asymmetric CH_2 deformation that is independent of crystallinity, which appears at around 1453 cm^{-1}, and the relative intensity 1227/1453 has been employed in many cases to estimate crystallinity [61,63,64]. The spectra highlighted in inset 2 of Fig. 10b, normalized to the intensity of the 1453 cm^{-1} band, clearly show higher crystallinity in the nanocomposites, correlating well with the calorimetry data. Finally, no evidence of bands due to the INTs were observed in the FITR spectra, nor was there any evidence for polymorphic behavior in the matrix, in agreement with the WAXD data.

3.7. *Mechanical and tribological properties*

Nanoindentation tests were performed on dried PHB/INT–WS_2 nanocomposite films. Fig. 11 shows graphs of nanohardness (H) and Young's modulus (E) of the PHB nanocomposites as a function of the INT content. The reported values of E and H were averaged over depths between 600 and 900 nm into the sample, where surface effects and imperfections are insignificant and both the E and H *versus* depth curves reach asymptotic values. At least 15 indentations were made at random locations on each film. A Poisson

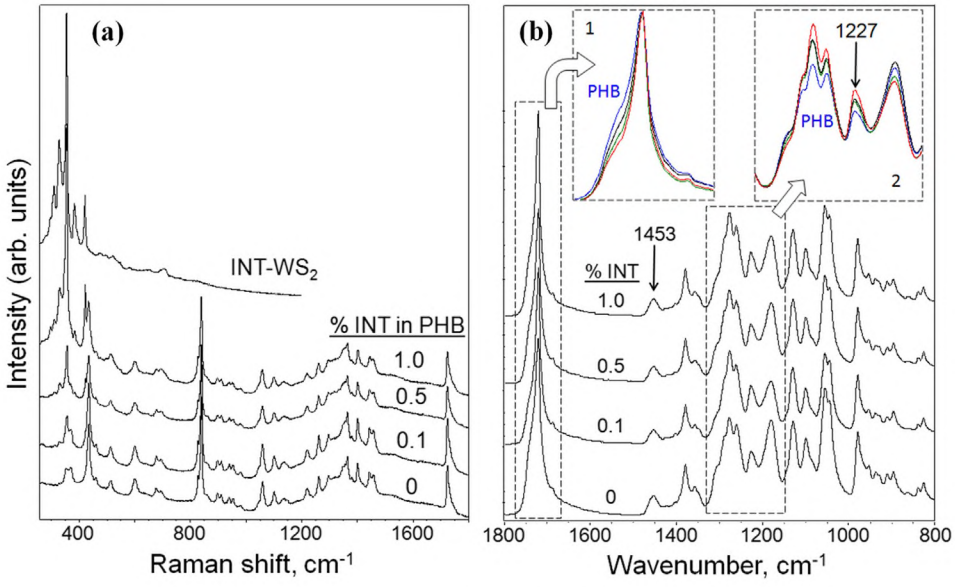

Fig. 10. (a) Raman and (b) infrared data from PHB/INT–WS_2 nanocomposites.

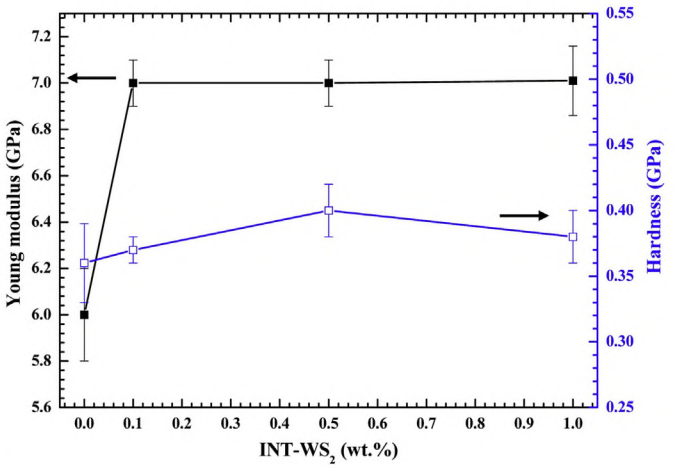

Fig. 11. Hardness and modulus from nanoindentation of PHB/INT−WS_2 nanocomposites.

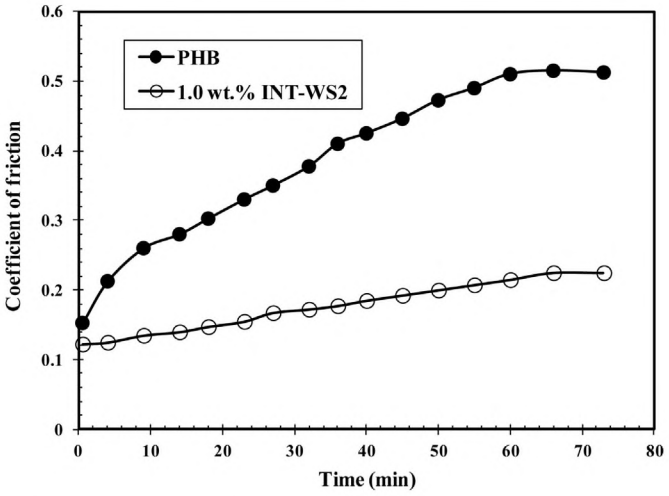

Fig. 12. Friction tests of PHB/INT−WS_2 nanocomposites; the test duration −73 min − corresponds to 1000 cycles.

ratio of 0.4 was used in the calculations. The Young's modulus of the pure PHB, around 6 GPa, increased upon the addition of only 0.1 wt.% of INT−WS_2 by ~17% to 7 GPa. However, this increment remained unchanged with increasing nanofiller concentrations. This trend is also apparent in the hardness variation but the increments in H in the nanocomposites with 0.1, 0.5 and 1.0 wt.% INT−WS_2 are noticeably lower (2−10%). The increase in hardness and modulus may arise from the deformation resistance induced by the INTs as a result of the improved crystallinity, reduced spherulites sized but could in principle decrease due to interspherulitic cracking.

Dry friction tests of these films were performed using a ball-on flat test. The friction coefficient and wear for pure PHB and a PHB/INT−WS_2 (1.0 wt.%) composite were compared. The roughness parameters of the PHB film with INT−WS_2 ($R_a = 49 \pm 4$ nm and $R_z = 296 \pm 22$ nm) were slightly larger than those for the neat film ($R_a = 43 \pm 0.2$ nm and R_z 260 ± 40 nm), attributed to the presence of the relatively stiff inorganic solid in the soft polymer matrix. The coefficient of friction (μ) represented the average of 5 measurements conducted at the mentioned conditions, with a value of $\mu = 0.15$ obtained for both matrices at the beginning of the run. After 1000 cycles μ for the neat PHB sample increased to 0.5, while that for the PHB film with nanotubes, $\mu = 0.2$, indicated only a minimal variation. The time evolution of μ for one of each type of sample is shown in Fig. 12.

In order to evaluate the wear after the tribological test, surface topography of the wear tracks was analyzed by atomic force microscope (AFM) before and after the friction measurements. The corresponding AFM images and profiles obtained along straight lines on the images of the wear tracks and neighboring out-of-track regions are shown in Fig. 13. It can be observed that the surface of the pure PHB film after the friction test suffered appreciably larger damage compared with that of the nanocomposite sample. The roughness R_a parameter was measured separately for in-track and out-of-track areas of each sample, using the AFM images. For instance, R_a for the out-of-track region is much lower for the neat PHB film than for that of the film with the INT−WS_2 (6 nm *versus* 24 nm), the roughness in the track on the PHB film increased to 48 nm whereas in the track of the film with INT−WS_2 it decreased to only 6 nm. One can also note the variance in the values of the R_a parameter measured by the AFM and the profilometer. This discrepancy can be attributed, among other reasons, to the significant difference in the scanning area of the AFM as compared to the measured surface area scanned by the profilometer as well as the different spatial resolution for the two measurements. The improved tribological properties of the films with INT−WS_2 can be attributed to strengthening of the film by the inorganic nanotubes and their possible exfoliation during friction and wear tests, which provided a lubricating layer on the rubbed surfaces.

4. Conclusions

The present investigation provides evidence for the efficient dispersion of inorganic nanotube-like INT−WS_2 in PHB, without the use of modifiers or surfactants. The INT−WS_2 nanofiller improves the crystallization behavior of PHB significantly when compared to other potential nano-sized fillers, such as carbon nanotubes and graphene, and specific nucleating agents, such as BN, melamine, thyamine, α-CD or lignine. The isothermal melt-crystallization of neat PHB and its nanocomposites was investigated at different crystallization temperatures and analyzed by the Avrami equation. It was found that the overall crystallization rates were reduced with an increase in the crystallization temperatures for both neat PHB and PHB/INT−WS_2 nanocomposites. Moreover, at a given crystallization temperature, the overall crystallization rates were faster in the nanocomposites than in neat PHB and increased further with an increase in the INT−WS_2 loading. However, the crystallization mechanism of PHB remained unchanged despite the crystallization temperature and INT−WS_2 loading. Both neat PHB and PHB/INT−WS_2 nanocomposites exhibited complex melting behavior after isothermal crystallization, without changing the equilibrium melting temperature of PHB. In addition, in the analysis of the activation energy of crystallization regime III of PHB/INT−WS_2 nanocomposites, it was determined that the value of fold surface free energy (σ_e) of PHB chains decreased with increasing INT−WS_2 content. All these results, along with a decrease in the free energy of nucleation decreased with the incorporation of INT−WS_2 into the matrix, demonstrate that INT−WS_2 is an effective nucleating agent for the crystallization of PHB. In the same way, the nonisothermal crystallization results indicate that INT−WS_2 exhibit higher nucleation efficiency in improving the crystallinity and crystallization rate of PHB. However, the presence of INTs has no impact on the crystalline structure of PHB. In addition, it was found that the nanohardness and Young's modulus of PHB were increased in the nanocomposites. For example, by adding only 0.1 wt.% of INT−WS_2 the Young's modulus increased by 17%. Similarly, the tribological properties of PHB were also improved

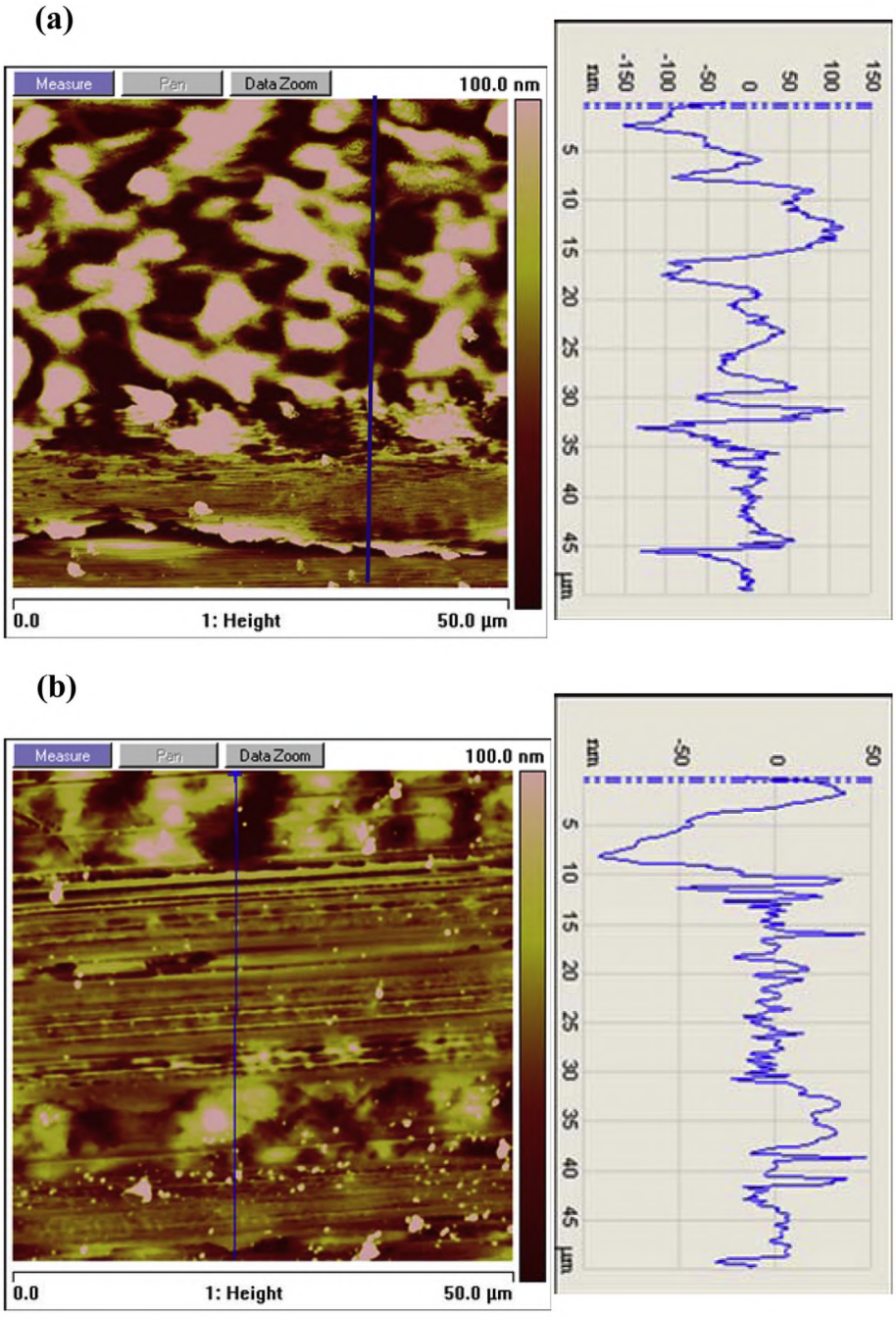

Fig. 13. AFM images and topography profiles of the wear tracks on the surface of (a) PHB film and (b) PHB/INT–WS_2 (1.0 wt.%).

with addition of INT–WS_2. The results reported herein are expected to be of great interest for the wider practical application of PHB.

Acknowledgment

This work was supported by the Spanish Ministry Economy and Competitivity (MINECO) (Project MAT-2010-21070-C02-01). MN would like to acknowledge the MINECO for a 'Ramón y Cajal' Senior Research Fellowship. The authors also wish to thank Isabel Muñoz of the ICTP Characterization Service for recording the Raman data.

References

[1] Y. Ikada, H. Tsuji, Macromol. Rapid Commun. 21 (2000) 117–132.
[2] R.A. Gross, B. Kalra, Science 297 (2002) 803–807.
[3] T. Keshavarz, I. Roy, Curr. Opin. Microbiol. 13 (2010) 321–326.
[4] L.S. Nair, C.T. Laurencin, Prog. Polym. Sci. 32 (2007) 762–798.
[5] V. Siracusa, P. Rocculi, S. Romani, D.M. Rosa, Trends Food Sci. Technol. 19 (2008) 634–643.
[6] P. Bordes, E. Pollet, L. Avérous, Prog. Polym. Sci. 34 (2009) 125–155.
[7] G.Q. Chen, Chem. Soc. Rev. 38 (2009) 2434–2446.
[8] A.J. Anderson, E.A. Dawes, Microbiol. Rev. 54 (1990) 450–472.
[9] T.V. Ojumu, J. Yu, B.O. Solomon, Afr. J. Biotechnol. 3 (2004) 18–24.
[10] A. El-Hadi, R. Schnabel, E. Straube, G. Muller, S. Henning, Polym. Test. 21 (2002) 665–674.
[11] H. Verhoogt, B.A. Ramsay, B.D. Favis, Polymer 35 (1994) 5155–5169.
[12] L. Yu, K. Dean, L. Li, Prog. Polym. Sci. 31 (2006) 576–602.

[13] C.H. Chan, C. Kummerlöwe, H.W. Kammer, Mater. Chem. Phys. 205 (2004) 664–675.
[14] C. Kinze, T. Freier, S. Kramer, K.P. Schmitz, J. Mater. Sci. Mater. Med. 13 (2002) 1051–1055.
[15] K. Weihua, Y. He, N. Asakawa, Y. Inoue, J. Appl. Polym. Sci. 94 (2004) 2466–2474.
[16] Y. He, Y. Inoue, J. Polym. Sci. Part B Polym. Phys. 42 (2004) 3461–3469.
[17] W. Kai, Y. He, Y. Inoue, Polym. Int. 54 (2005) 780–789.
[18] J. Quian, L. Zhu, J. Zhang, R.S. Whitehouse, J. Polym. Sci. Polym. Phys. 45 (2007) 1564–1577.
[19] D. Briassoulis, J. Polym. Environ. 14 (2004) 289–307.
[20] G.J.M. de Koning, P.J. Lemstra, Polymer 34 (1993) 4089–4094.
[21] P. Maiti, C.A. Batt, E.P. Giannelis, Biomacromolecules 8 (2007) 3393–3400.
[22] S.F. Hsu, T.M. Wu, C.S. Liao, J. Polym. Sci. Part B Polym. Phys. 45 (2007) 995–1002.
[23] C. Xu, Z. Qiu, J. Polym. Sci. Part B Polym. Phys. 47 (2009) 2238–2246.
[24] X., Jing, Z. Qiu, J. Nanosci. Nanotechnol. 12 (2012) 7314–7321.
[25] R. Tenne, L. Margulis, M. Genut, G. Hodes, Nature 360 (1992) 444–445.
[26] L. Margulis, G. Salitra, R. Tenne, M. Talianker, Nature 365 (1993) 113–114.
[27] A. Zak, L. Sallacan-Ecker, A. Margolin, M. Genut, R. Tenne, Nano 4 (2009) 91–98.
[28] A. Zak, L. Sallacan Ecker, N. Fleischer, R. Tenne, Sens. Transducers J. 12 (2011) 1–10.
[29] M. Naffakh, A.M. Díez-Pascual, C. Marco, G. Ellis, M.A. Gómez-Fatou, Prog. Polym. Sci. 38 (2013) 1163–1231.
[30] E. Zohar, S. Baruch, M. Shneider, H. Dodiu, S. Kenig, D.H. Wagner, A. Zak, A. Moshkovith, L. Rapoport, R. Tenne, Sens. Transducers J. 12 (2011) 53–65.
[31] C.S. Reddy, A. Zak, E. Zussman, J. Mater. Chem. 21 (2011) 16086–16093.
[32] G. Lalwani, A.M. Henslee, B. Farshid, P. Parmar, L. Lin, Y.X. Qin, F.K. Kasper, A.G. Mikos, B. Sitharaman, Acta Biomater. 9 (2013) 8365–8373.
[33] M. Naffakh, M. Remškar, C. Marco, M.A. Gómez, I. Jiménez, J. Mater. Chem. 21 (2011) 3574–3578.
[34] M. Naffakh, C. Marco, G. Ellis, Cryst. Eng. Commun. 16 (2014) 1126–1135.
[35] P.J. Barham, J. Mater. Sci. 19 (1984) 3826–3834.
[36] R.E. Withey, J.N. Hay, Polymer 40 (1999) 5147–5152.
[37] M.L. Di Lorenzo, P. Sajkiewicz, A. Gradys, P. La Pietra, E-Polymers (2009) 1–12.
[38] L.M.W.K. Gunaratne, R.A. Shanks, Eur. Polym. J. 41 (2005) 2980–2988.
[39] M. Avrami, J. Chem. Phys. 7 (1939) 1103–1112.
[40] M. Avrami, J. Chem. Phys. 8 (1940) 212–224.
[41] M. Avrami, J. Chem. Phys. 9 (1941) 177–184.
[42] J.N. Hay, Br. Polym. J. 3 (1971) 74–82.
[43] R.A. Shanks, L.M.W.K. Gunartne, J. Therm. Anal. Chem. 104 (2011) 1117–1124.
[44] J.D. Hoffman, J.J. Weeks, J. Res. Natl. Bur. Stand. A 66 (1962) 13–28.
[45] J.L. Lauritzen, J.D. Hoffman, J. Appl. Phys. 44 (1973) 4340–4352.
[46] J.D. Hoffman, G.T. Davies, J.J. Lauritzen, in: N.B. Hannay (Ed.), Treatise on Solid State Chemistry, vol. 3, Plenum Press, New York, 1976.
[47] P.J. Barham, A. Keller, E.L. Otun, J. Mater. Sci. 19 (1984) 2781–2794.
[48] R. Pearce, G.R. Brown, R.H. Marchessault, Polymer 35 (1994) 3984–3989.
[49] J.D. Hoffman, R.L. Miller, Polymer 24 (1983) 3–26.
[50] M. Yokouchi, Y. Chatani, H. Tadokoro, K. Teranishi, H. Tani, Polymer 14 (1973) 267–272.
[51] P. Pan, Y. Inoue, Prog. Polym. Sci. 34 (2009) 605–640.
[52] Y.Q. Zhu, W.K. Hsu, N. Grobert, B.H. Chang, M. Terrones, H. Terrones, H.W. Kroto, D.R.M. Walton, B.Q. Wei, Chem. Mater. 12 (2000) 1190–1194.
[53] M. Staiger, C. Thomsen, G. Radovsky, H. Telg, P. Rafailov, K. Gartsman, A. Zak, Phys. Rev. B 86 (2012) art. no. 165423.
[54] M. Virsek, A. Jesih, I. Milosevic, M. Damnjanovic, M. Remskar, Surf. Sci. 601 (2007) 2868–2872.
[55] P.M. Rafailov, C. Thomsen, K. Gartsman, I. Kaplan-Ashiri, R. Tenne, Phys. Rev. B 72 (2005) art. no. 205436.
[56] C. Schuffenhauer, G. Wildermuth, J. Felsche, R. Tenne, Phys. Chem. Chem. Phys. 6 (2004) 3991–4002.
[57] H. Sato, R. Murakami, K. Mori, Y. Ando, I. Takahashi, I. Noda, Y. Ozaki, Vib. Spectrosc. 51 (2009) 132–135.
[58] H. Sato, Y. Ando, J. Dybal, T. Iwata, I. Nosa, Y. Ozaki, Macromolecules 41 (2008) 4305–4312.
[59] Q. Wu, G. Tian, S.Q. Sun, I. Noda, G.Q. Chen, J. Appl. Polym. Sci. 82 (2001) 934–940.
[60] A. Padermshoke, Y. Katsumoto, H. Sato, S. Ekgasit, I. Noda, Y. Ozaki, Polymer 245 (2004) 6547–6554.
[61] M. Kansiz, A. Domínguez-Vidal, D. McNaughton, B. Lendl, Anal. Bioanal. Chem. 388 (2007) 1207–1213.
[62] J. Xu, B.H. Guo, R. Yang, Q. Wu, G.Q. Chen, Z.M. Zhang, Polymer 43 (2002) 6893–6899.
[63] L. Garrido, I. Jiménez, G. Ellis, P. Cano, J.M. García-Martínez, L. López, E. de la Peña, J. Appl. Polym. Sci. 119 (2011) 3286–3296.
[64] G. Ellis, P. Cano, M. Jadraque, M. Martín, L. López, T. Núñez, E. de la Peña, C. Marco, L. Garrido, Anal. Bioanal. Chem. 399 (2011) 2379–2388.